Journal of Hydrology: Regional Studies 59 (2025) 102266

Contents lists available at ScienceDirect

Journal of Hydrology: Regional Studies

journal homepage: www.elsevier.com/locate/ejrh

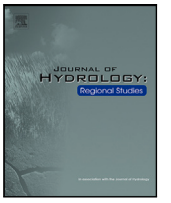

Data-driven assessment of climate change and vegetative cover dynamics in traditional oases

Elisa Baioni, Giulia Fiantanese, Giovanni Michele Porta *

Department of Civil and Environmental Engineering, Politecnico di Milano, Piazza Leonardo da Vinci, Milan, 20133, Italy

ARTICLE INFO

Dataset link: https://data.mendeley.com/preview/gcx5hkfb5k?a=07bddc9c-f3db-47c9-823c-894d869c8232

Keywords:
Climate change
Satellite imagery analysis
Vegetation dynamics
Traditional oases
Time series modeling
Data driven models
Uncertainty quantification

ABSTRACT

Study region: Abiod Valley, Aurès region, Algeria.
Study focus: This work focuses on the relation between climatic forcing and vegetation cover dynamics in traditional oases. This study pursues two main objectives: (1) estimate the vegetative surface cover of traditional oases from satellite images, (2) quantify the impact of climatic variables on vegetation dynamics and assess future scenarios. We propose a methodology that leverages satellite imagery and derived indices (NDVI, NDMI) to quantify vegetation cover and water stress events at the oasis spatial scale. We then assess the feedback between climate and vegetation cover at monthly and yearly scale through multivariate analyses based on vector autoregression (VAR) and vector error correction (VEC) models.
New hydrological insights for the region: Our findings reveal an appreciable decrease in vegetation cover over the last decade across three considered traditional oases in the study region. The monthly scale analysis suggests a lagged effect of climatic variables, especially cumulative precipitation, on vegetation water stress. The long term VEC prediction of climatic variables aligns with GDDP-CMIP6 climate projections, forecasting an increase in average temperature and potential evapo-transpiration. A significant decline in vegetative surface cover is predicted by 2050 from the analysis of yearly data, highlighting the critical need for water management interventions to safeguard oasis ecosystem and prevent desertification.

1. Introduction

In arid climatic regions, vegetation cover serves as a fundamental element for ecological stability, particularly within oasis ecosystems which are highly sensitive (Chen et al., 2024; Lin et al., 2009) and particularly exposed to global warming effects. The traditional oases of North Africa represent a recognized agro-forestry system, providing key ecosystem services to local communities, including provisioning, regulating, and cultural services (Santoro, 2023). In the current climatic and socio-economic scenario, these systems face significant vulnerabilities (Dhawi and Aleidan, 2024, and references therein). In this context, water management is a key factor (Chen et al., 2024; Santoro, 2023). Detecting temporal changes in vegetation cover and quantifying the contribution of climatic factors can be crucial to assess the risk of desertification and formulate adequate adaptation measures.

Satellite-derived vegetation are widely used as an effective method for monitoring and assessing vegetation across diverse ecosystems and landscapes (Levin et al., 2007; Wallace et al., 2006). The normalized difference vegetation index (NDVI) is one of the most widely used tools for monitoring vegetation health due to its reliance on long-term satellite data readily available at low cost (Huang et al., 2021). NDVI quantifies vegetation greenness and vigor by analyzing the difference between near-infrared (NIR) and red light reflectance. This index has proven valuable in ecosystem and cropland monitoring (Li et al., 2019; Filgueiras et al.,

* Corresponding author.
E-mail address: giovanni.porta@polimi.it (G.M. Porta).

https://doi.org/10.1016/j.ejrh.2025.102266
Received 20 September 2024; Received in revised form 17 February 2025; Accepted 20 February 2025
Available online 13 March 2025

2019; Boori et al., 2020; Yu et al., 2004), and for monitoring vegetation dynamics in oasis systems (Lin et al., 2009). Additionally, the normalized difference moisture index (NDMI) (Gao, 1996) provides valuable insights into vegetation water content and stress levels. Derived from satellite imagery as normalized reflectance difference between near-infrared (NIR) and short-wave infrared (SWIR) bands, NDMI has proven effective in monitoring moisture conditions, water stress, and drought events (Lin et al., 2011; Wilson and Sader, 2002; Hayes et al., 2008). NDVI and NDMI are positively correlated, highlighting the link between land surface moisture and vegetation dynamics (Lin et al., 2009). This combined analysis of NDVI and NDMI is particularly significant for assessing vegetation dynamics and detecting drought, especially in oasis landscapes.

Our aim is to link detected oases vegetative dynamic patterns, as rendered by NDVI and NDMI analyses, to climatic trends by using simplified data-driven approaches. Statistical correlation between vegetative cover dynamics and climate data in arid areas has been explored in numerous studies (Mo et al., 2019; Liu et al., 2021). Our specific goal is to exploit such correlation to build site-specific data-driven predictive models linking climatic trends to the vegetative cover surface area and water stress detected at the scale of a single oasis. To these ends we chose to employ regression models, as they offer a relatively easy-to-implement solution. These approaches serve as linear predictors and provide interpretable coefficients that can be used to quantify the mutual correlation and importance (or sensitivity) of the considered variables. A key feature of our analysis is that the proposed approaches allow identifying and propagating uncertainties in modeling predictions casting the analysis in a probabilistic framework. In this work we select two approaches to time series modeling, namely Vector Autoregression (VAR) and Vector Error Correction model (VEC). VAR is a powerful way to extract past and future movements of multiple interrelated endogenous variables. It extends univariate autoregressive models to multivariate time series and offers wide application flexibility. VAR models have been successfully applied to a broad range of data, from economics and finance (Awokuse and Bessler, 2003; Clements and Mizon, 1991) to climatic variables (Adenomon et al., 2013; Nuruzzaman et al., 2023; Kleiber et al., 2013; Ferdous et al., 2011). VEC model is an extension of VAR including an error correction term to account for cointegrations and long-term relations among variables. Unlike VAR, the VEC model can handle non-stationary variables with cointegration, making it a valuable tool for analyzing data across various fields. The VEC approach has seen successful applications in many fields such as economic (Honkatukia et al., 2008; Thoenes, 2014), environmental (Fahria and Sulistiana, 2021; Kaur et al., 2021) and climatic studies (Stephenson et al., 2023; Sudheesh and Subramanian, 2022).

Our key objective is here a methodology to assess the past and future trajectory of traditional oases systems. This work thus features the following key novelties: (i) define a robust data analysis methodology, specifically tailored to the assessment of oasis vegetative cover surface area based on NDVI and NDMI indices, by combining diverse remote sensing datasets, (ii) introduce and benchmark the application of VAR and VEC models in the assessment of water stress and vegetative cover dynamics in traditional oases. Our analysis considers the feedback between climatic variables and oases vegetative dynamics at two separate time scales. A monthly time scale is considered to assess the impact of the climatic factors on the vegetation water stress level. Annual data are employed to model the long-term oasis's vegetative cover dynamics alongside climatic variables, allowing for future scenario predictions. The methodology is applied to oasis systems in the Wadi Aboid watershed, Aures region, Algeria, in line with the objectives of the AMAZING (Atlas Mountains, Aurès Zone, INterconnecting local sciences and Global challenges) project (AMAZING, 2023). The decline of the traditional oases in the Aureѐ region is observable on the ground but has never been quantified directly. In particular, this oasis system is challenged by climatic factors and by a gradual decline in maintenance of date palm groves, which constitute the main vegetation cover in the oasis. Through the application of our proposed methodology we aim to provide quantitative evidence of the temporal evolution of the oasis vegetative dynamics and to assess its possible future trajectory.

The paper is structured as follows: Section 2 describes the methodology used to address the estimate of the vegetative surface (Section 2.2) and the modeling and future projections of the climatic and vegetative variables (Section 2.4). The study area is presented in Section 3 while the key findings are discussed in Section 4. The conclusions drawn from our study are reported in Section 5.

2. Methodology

This study pursues three main objectives: (1) detecting temporal variations in the oasis vegetative surface cover, (2) identifying the key climatic drivers influencing vegetative surface changes and their correlation, (3) predicting future scenarios to plan strategic interventions for preventing oasis desertification.

The first goal is achieved by analyzing satellite imagery of the study area spanning the past four decades. Details on the employed methodology can be found in Section 2.2. Section 2.3 complements the analysis with a method to evaluate water stress in the oasis. The results derived from objective (1) along with the historical climatic data are used to build a statistical model to quantify the correlations between input variables and the impact of climatic factors on the oasis extent variation. The methodology employed to achieve objectives (2)-(3) is provided in Section 2.4. The model is then utilized to predict future values of the assessed quantities, along with a quantification of the associated uncertainties.

2.1. Input data and preprocessing

Oasis' vegetation surface estimation leverages multiple remote sensing datasets, as reported in Table 1. To delineate the vegetation extent, Sentinel-2 satellite imagery (Dechoz et al., 2015) is taken as a reference. This choice is motivated by the higher spatial, temporal and spectral resolution of Sentinel-2 imagery compared to Landsat 8 (Ihlen, 2019). Additionally, Sentinel-2 offers greater accuracy in land cover and vegetation identification (Isioye et al., 2020; Al-Gaadi et al., 2016). We used the satellite imagery

Table 1
Dataset: Satellite images and climatic data.

Data type	Dataset	Provider	Spatial resolution	Time range
Satellite images	Sentinel 2[a]	Copernicus/SOAR	10 m	2016–2023
Satellite images	Landsat 8[b]	NASA/USGS	30 m	2013–2023
Satellite images	Landsat 5[c]	NASA/USGS	30 m	1984–2012
Climate data (precipitation, temperature, solar radiation)	ECMWF/ERA5_LAND[d]	Copernicus	11132 m	1950–2022
Climate data (relative humidity, wind speed)	AgERA5 (ECMWF)_LAND[e]	Copernicus	9600 m	1979–2024
Climate data	NEX-GDDP-CMIP6[f]	NASA	27830 m	1950–2100

[a] https://soar.earth/satellites/sentinel.
[b] https://developers.google.com/earth-engine/datasets/catalog/LANDSAT_LC08_C02_T1_L2.
[c] https://developers.google.com/earth-engine/datasets/catalog/LANDSAT_LT05_C02_T1_L2.
[d] https://developers.google.com/earth-engine/datasets/catalog/ECMWF_ERA5_LAND_DAILY_AGGR.
[e] https://gee-community-catalog.org/projects/agera5_datasets/.
[f] https://developers.google.com/earth-engine/datasets/catalog/NASA_GDDP-CMIP6.

sourced from the SOAR website, which identify vegetative cover. These images have a 10-meter resolution but encompass a limited time interval, ranging from 2016 to 2022. To assess the oasis area variation across a longer time window, Landsat 5 (Sayler, 2020) and Landsat 8 satellite imagery were employed, the latter covering the time intervals 1985–2011 and 2013–2023, respectively. Landsat datasets provide atmospherically corrected surface reflectance and land surface temperature derived from the TM sensor (Landsat 5) and the OLI/TIRS sensors (Landsat 8). Section 2.2 details the procedure employed for identifying the oasis area.

The climatic data (precipitation, temperature, solar radiation, wind speed, relative humidity) employed to assess climate within the study area originate from the ECMWF ERA5-Land (precipitation, temperature, solar radiation) (Muñoz Sabater, 2019) and AgERA5 (ECMWF) (wind speed, relative humidity) datasets (Copernicus, 2017). ERA5-Land offers a reanalysis dataset, providing a consistent perspective on the evolution of land variables from 1950 to 2022 with hourly temporal resolution. Reanalysis combines model data with observations into a global and consistent dataset. The AgERA5 (ECMWF) dataset provides daily surface meteorological data from 1979 to present based on the hourly ECMWF ERA5 data at surface level.

The climate change data used for comparison with the predictions derived from our model are sourced from the NEX-GDDP-CMIP6 dataset (Thrasher et al., 2012). This dataset comprises global downscaled climate scenarios derived from the General Circulation Model (GCM) simulations conducted under the Coupled Model Intercomparison Project Phase 6 (CMIP6).

The solar radiation, wind speed, relative humidity are used to compute the evapotranspiration according to the Penman-Monteith equation (Zotarelli et al., 2010)

$$ET_0 = \frac{0.408\Delta\left(R_n - G\right) + \gamma\frac{900}{T+273}u_2\left(e_s - e_a\right)}{\Delta + \gamma\left(1 + 0.34u_2\right)} \tag{1}$$

where ET_0 is the reference evapotranspiration rate [mm d^{-1}], T the mean air temperature [°C], u_2 the wind speed [m s^{-1}] at 2 m above the ground, R_n the solar net radiation [MJm^{-2}d^{-1}], G the soil heat flux density [MJm^{-2}d^{-1}], e_s the saturation vapor pressure [kPa], e_a the actual vapor pressure [kPa], Δ the slope of the saturated vapor pressure curve [kPa], and γ the psychometric constant [kPa°C^{-1}].

2.2. Vegetation cover analysis

The analysis of the vegetative surface cover of the study area is carried out upon relying on the Normalized Difference Vegetation Index (NDVI) (Huang et al., 2021; Rouse et al., 1973). The index is correlated with the vegetation crown density. NDVI is calculated as the ratio between top of the atmosphere (TOA) reflectance of a red band (RED) around 0.66 micron and a near-infrared band (NIR) around 0.86 micron.

$$NDVI = \frac{NIR - RED}{NIR + RED} \tag{2}$$

The NDVI ranges from −1 to 1, serving as a proxy for vegetation health and density. Low values indicate bare soil while high values represent dense vegetation. Here we assume that the considered spatial domain lacks vegetation, except for the oasis area. NDVI is used to estimate the oasis' area by distinguishing the oasis from non-vegetated surfaces. A threshold value of the index τ_{NDVI} is then necessary to perform the calculation. The value of τ_{NDVI} is determined by comparing the NDVI map derived from Landsat 8 to those from Sentinel-2 provided by the website SOAR, the latter showing the vegetative surface for an optimal NDVI threshold. The NDVI index from the Landsat imagery has been calculated by processing the satellite images in Google Earth Engine. The computation of the optimal threshold to identify the vegetative surface of the oasis is performed in Matlab by the following procedure:

1. **Mask from Sentinel-2 imagery**: a mask of the vegetative surface M_S is created from Sentinel-2 imagery relying upon Otsu's algorithm (Otsu et al., 1975). The Otsu method is commonly used to select the optimal global threshold to obtain the vegetation cover thresholds and has been previously applied for oases' identification. This algorithm is implemented in Matlab by the *graythresh* function, which computes a global threshold from a grayscale image by minimizing the intraclass variance of the thresholded black and white pixels;

2. **Resize Landsat imagery**: the Landsat satellite images are resized by the Matlab function *imresize* to ensure an exact overlap between Landsat and Sentinel imagery;
3. **Optimal threshold identification**: the optimal threshold value of the NDVI (τ^*) for each Landsat image is identified as the threshold value (τ) that maximizes similarity between the masks obtained from Landsat and Sentinel datasets. The value τ^* is computed through an iterative process where τ is incremented at each iteration i over the set $[-1, 1]$. The iterative procedure comprises the following steps:

   (a) **Mask from Landsat imagery**: for each iteration i a mask M_{L_i} is generated from the image $image_L$ considering the threshold τ_i

   $$M_{L_i} = image_L > \tau_i \tag{3}$$

   (b) **Evaluation of similarity**: the similarity (sim) between the masks obtained from the two datasets, M_S and M_L, is quantified as

   $$sim_i = \frac{N_p(M_L = M_S)}{N_{tot}} \tag{4}$$

   where $N_p(M_L = M_S)$ represents the number of pixels of M_L that coincide with those in M_S, N_{tot} is the total number of pixels of the mask, with $N_{tot}(M_L) = N_{tot}(M_S)$.

The optimal NDVI threshold value τ^* for each satellite image is identified as the τ_i value that maximizes sim_i.

Section S1 of the Supplementary Material exemplifies the application of the method to a practical case. The procedure is iterated monthly from 2016 to 2023. For each month, a satellite image with minimal cloud cover, offering good surface visibility, is selected from each dataset, prioritizing images captured on the same day if available. To remove the impact of the seasonal variations in NDVI caused by vegetation dynamics and environmental factors, the average monthly threshold (τ^*_m) is calculated for each year. Subsequently, the minimum and maximum τ^*_m values across the entire time frame are considered to account for uncertainty on the estimate of the threshold of the NDVI. Both τ^*_{min} and τ^*_{max} are used to quantify the vegetative cover surface A_v, maximum and minimum area respectively, from Landsat 5 and Landsat 8.

2.3. Vegetation water stress

The Normalized Difference Moisture Index ($NDMI$) has been evaluated for monitoring water stress in plants. $NDMI$ is calculated using the near-infrared (NIR) and the short-wave infrared ($SWIR$) reflectance as (Gao, 1996)

$$NDMI = \frac{NIR - SWIR}{NIR + SWIR} \tag{5}$$

$NDMI$ ranges from −1 to 1 its value being proportional to moisture levels. This study leverages $NDMI$ to identify areas within the oasis that have experienced water stress over the last decades. For each satellite image, we compute a $NDMI$ threshold as the 10th percentile of positive $NDMI$ values, denoted as $\tau_{10} = p_{10}(NDMI|NDMI > 0)$, i.e. considering a conditional probability distribution of positive NDMI values. Negative values are excluded as they are assumed to be related to bare soil cover. The average value of τ_{10} is determined at monthly scale and used to estimate the regions within the study area experiencing the most significant water stress A_s, defined as the area with NDMI values lower than τ_{10}. The quantity R_{ws}, obtained by normalizing A_s by the area of the vegetative mask used for the computation, is employed to construct a statistical model that aims to identify the primary influencing factors on R_{ws} and predict potential future values. This modeling step is detailed in Section 2.4.

2.4. Data driven models

We leverage data-driven approaches to determine future trends and events based on current and historical observations. In this study a multivariate statistical model is employed to assess the interplay between climatic variables and vegetative surface changes within the study area and to predict their potential future values. The model is constructed using:

1. Historical climatic data for the study area obtained from the ERA5 reanalysis dataset (see Table 1 for details). Considered data include cumulative precipitation P_c, mean temperature T, and mean evapotranspiration ET_0, given their significant influence on vegetation changes and water stress;
2. Temporal variations in vegetative surface area A_v and water-stress areas R_{ws} of the oasis, derived from the analysis described in Section S1 of Supplementary Material.

The analysis is conducted at two distinct temporal scales: (1) annual scale to assess the long term impact of climatic variables on the variation of the vegetative surface area, (2) monthly scale to investigate the oasis's area subjected to water stress with higher temporal resolution. To ensure consistency across both analyses, the chosen time intervals reflect the availability of both climatic data and satellite imagery. The annual analysis spans from 1985 to 2022, while the monthly analysis covers the period from 2014 to 2022.

Prior to model selection, preliminary tests are performed to assess the stationarity of the time series and identify any potential cointegrations between the variables. This step ensures the choice of the most appropriate statistical model for the underlying data characteristics. All analyses were performed using the R statistical software package (R. Core Team et al., 2016). The Autoregressive Vector (VAR) model is suitable for stationary data at level (in its original form). When the input variables are not stationary at level but their first differences are stationary and exhibit cointegration, the Vector Error Correction model (VEC) becomes an appropriate choice.

The initial step involves evaluating the stationarity properties of the time series data. The Augmented Dickey–Fuller (ADF) test (Banerjee et al., 1993) is employed to detect the presence of a unit root, which indicates non-stationarity (see Section S2 in Supplementary Material). The test relies upon the computation of t-statistics from a regression equation of the variable x which incorporates a constant, a linear trend and a number of lags equal to $\mathrm{trunc}((length(x)-1)^{1/3})$. Based on the derived p-value the test determines whether the null hypothesis (existence of a unit root, i.e. non-stationary time series) is satisfied.

If the data exhibits non-stationarity at the level, we proceed to investigate cointegration. Cointegration is identified using the Johansen test (Johansen, 1988; Johansen and Juselius, 1990) and assesses the existence of long-term relationships between the variables. Moreover, the analysis determines the cointegration rank, indicating the number of such equilibrium relationships that are detected. Further details on the test are provided in Section S3 in Supplementary Material.

The number of lags (q) included in the model significantly influences the accuracy of the results, particularly in the VEC model. The lag length reflects the time it takes for a variable to be impacted by its own past values and by the past values of other variables in the model. The optimal lag length to be considered in the multivariate time series analysis is identified relying upon the AIC criterion. AIC is calculated from the maximum likelihood (L) and the number of estimated parameters (n) of the model as (Sakamoto et al., 1986)

$$AIC = 2n - 2ln(L) \tag{6}$$

When comparing models fitted by maximum likelihood to the same data, the smaller the AIC the better the fit. AIC can be used to estimate the posterior probability associated to each of the N_M available alternative interpretive models as (Janetti et al., 2012)

$$p(M_k \mid \mathbf{X}^*) = \frac{\exp(-\frac{1}{2}\Delta AIC_k)p(M_k)}{\sum_{i=1}^{N_M}\exp(-\frac{1}{2}\Delta AIC_i)p(M_i)} \tag{7}$$

where X^* are the predicted endogenous variables, $\Delta AIC_k = AIC_k - min\{AIC_k\}$ with AIC_k corresponding to the AIC value of the model M_k, and $p(M_i)$ is the prior probability associated with the model M_k. Without prior information, $p(M_i)$ can be assumed equal to $1/N_M$. The posterior model probabilities in Eq. (7) allow to (1) rank a set of candidate models in terms of their associated posterior probabilities, and (2) quantify the uncertainty associated with the model predictions by assigning a weight to each model based on its posterior probability. The constructed models are used to analyze the relationships between the endogenous variables and to predict their possible future values. The statistical models used for each time scale are specified below.

2.4.1. Modeling of stationary variables

If the ADF test indicates stationarity, the VAR model is employed. The model extends the idea of univariate autoregression to k time series regressions to capture the interdependencies among them. The VAR model of lag order q is formulated as (Hamilton, 2020)

$$y_t = A_1 y_{t-1} + \cdots + A_q y_{t-q} + C D_t + u_t \tag{8}$$

where, y_t is a $k \times 1$ vector of endogenous variables, A_j with $j = 1, \ldots, q$ the coefficient matrices of dimension $k \times k$, D_t represents the deterministic regressors, and C is the corresponding coefficient matrix, and u_t indicates the $k \times 1$ vector error assumed to be normally distributed with mean zero and variance $\Sigma_u = E(u_t' u_t)$. The deterministic regressors term accounts for centered seasonal dummy variables and/or exogenous variables and can be expressed as a linear trend or a constant (including zero). The $k^2 \times q$ coefficients of the matrix A and the $n \times k$ constants of the deterministic regressor, if any, are estimated by ordinary least squares (OLS) for each equation separately. Seasonality from monthly data is incorporated into the model using seasonal dummy variables treated as external factors (exogenous). Each dummy variable takes a value of 1 during its corresponding month and 0 otherwise. This approach adds 11 coefficients to the VAR model, capturing seasonality without introducing perfect multicollinearity.

2.4.2. Modeling of non-stationary variables

When the ADF test indicates non-stationarity, the existence of cointegration is verified using the Johansen test.

In this case, a VEC model is employed. The VEC model combines a VAR model with error correction terms, enabling it to capture both the short-term effects between variables and the long-term effects of time series data. The general form of VEC for k endogenous variables with order q and cointegration rank r, with $r \leq k$, is (Hamilton, 2020)

$$\Delta y_t = \Pi y_{t-1} + \sum_{i=1}^{q-1} A_i \Delta y_{t-i} + \mu + C D_t + u_t \tag{9}$$

where Δ indicates differentiation, $\Delta y_t = y_t - y_{t-1}$, y_{t-1} the vector endogenous variable with $lag = 1$, Π the coefficient matrix of cointegrating relationships, A_i the $k \times k$ matrix coefficient of each endogenous variable i, measuring transient effects, D_t the $k \times 1$

vector of deterministic terms and C the corresponding coefficient matrix, u_t the $k \times 1$ error vector with zero mean and variance–covariance matrix $\Sigma_u = E(u_t' u_t)$, μ a constant term. The Π matrix can be written as $\alpha\beta'$ where β is the $k \times r$ cointegration matrix containing information on the equilibrium relationships between the variables in levels, and α represents the $k \times C$ loading matrix describing the speed at which a dependent variable converges back to its equilibrium value. The r value corresponds to the rank of the matrix Π determined according to the Johansen test. The cointegration term may include a constant or a trend in the cointegration equations according to the data. The model coefficients are estimated using the Maximum Likelihood (ML) method.

Note that the VEC formulation in Eq. (9) and VAR Eq. (8) differ in two key aspects. First, the VEC includes a cointegration term to account for long-run equilibrium relationships, which is absent in the VAR. Second, the VEC is formulated in first differences, while the VAR uses levels of the variables. To obtain fitted and predicted values in their original level form (instead of first differences as resulting from Eq. (9)) the *vec2var* function implemented in R (Pfaff and Taunus, 2007; Lütkepohl, 2005) is employed. This function effectively transforms a VEC model into a level-VAR form preserving the cointegration information within the structure of the VAR.

2.5. Model suitability

Various tests are performed to evaluate the adequacy of the constructed model in terms of stability, residual autocorrelation, nonnormality and heteroskedasticity.

Model stability is assessed by calculating the eigenvalues of the coefficient matrix in Eqs. (8)–(9). Here the stability is intended as the stability of the system of difference equations. If the moduli of the eigenvalues of A are less than 1 the model is stable (Pfaff and Taunus, 2007). Normality of residuals is not a necessary condition for model validity. However, non-normality of the residuals may indicate other model deficiencies such as nonlinearities or structural change (Lütkepohl, 2013). The Jarque–Bera normality test is employed to test if the residuals are normally distributed. Further details are provided in Section S4 in Supplementary Material. The lack of serial correlation in the model residuals is tested by the Portmanteau test and the LM test proposed by Breusch and Godfrey (Breusch, 1978; Edgerton and Shukur, 1999) (see Section S5). Correlation in residuals may lead to unreliable parameters estimation and inaccurate prediction.

The heteroskedasticity is assessed relying upon the ARCH test (Lütkepohl, 2005) (see Section S6 in Supplementary Material). Heteroskedastic residuals can indicate structural change, implying instability of the regression coefficients. In this regard, the stability of the regression relationships in the model is evaluated by an empirical fluctuation process estimated for each regression. Specifically, we refer to the CUSUM (Cumulative Sum) processes, which contain cumulative sums of standardized residuals. Further details can be found in Kleiber (2002). A stable fluctuation process remains within the critical bounds and close to zero.

After model construction and validation, the forecast error variance decomposition (FEVD) can be used to analyze how a shock to one variable affects the others. FEVD quantifies the contribution of each variable to the overall forecast error variance in the multivariate model. This helps identify which variables have the most significant influence on the uncertainty associated with future predictions. Details on FEVD are provided in Section S7 of the Supplementary Material.

3. Study area

M'Chouneche, an Algerian commune nestled within the Oued Labiod Watershed of Biskra Province, features a traditional oasis, as visible in Fig. 1. The area is located at an elevation exceeding 300 meters above sea level. The town hosts a community of over 7000 inhabitants which has historically maintained a rich ecosystem of approximately 93,000 palm trees (Medouki et al., 2022). The oasis falls within the drainage basin of Oued el Hai Biskra with headwaters originating in the Belezma Mountains, which receive 400-500 mm/year of precipitation, and flowing northeasterly for roughly 60 km through the Aurès region before emerging onto the El Outaya Plain (Fiantanese, 2023). M'Chouneche experiences a classic desert climate with distinct seasonal variations. Winters are mild, featuring pleasant days (13-25°C) and cool nights (5-8°C). However, summers stand in stark contrast, characterized by intense heat with temperatures frequently exceeding 40°C.

The oasis of M'Chouneche belongs to traditional wadi oases: the villages and the palm grove are located along the wadi. M'Chouneche oasis supports a variety of plant life that is well-adapted to the desert environment. The vegetation is dominated by date palm trees (see Fig. 2), which are a common feature in desert gardens and play a crucial role in the ecosystem of the oasis. This vegetation not only sustains the local population with food and shade but also contributes significantly to the socio-environmental well-being of the area.

Our aim is here to apply the methodology proposed in Section 2 to assess the long term trends in the aerial extension of M'Chouneche oasis, as well as the short term dynamics of water stress. Climatic variables can be a direct or indirect cause of deterioration of the oasis environment. Climate fluctuations at small and large temporal scales can directly induce water stress, thus impacting vegetation density and extension. At the same time the increase in temperature and disruption of precipitation patterns that has been observed in the last decade creates the conditions for abandonment and lack of management and maintenance of small scale plantations, that was traditionally provided by the local community. Management of small wadi oasis traditionally relies on surface water resources, this management model being more prone to failure due to climate change, as opposed to large industrial date palm tree plantations existing in the region of Biskra (Algeria) that have been largely developed relying entirely on deep groundwater resources (Petit et al., 2017). The development of such large-scale modern oases systems may be another cause of abandonment of traditional oases systems, becoming less economically viable due to scarcity of water. In the current scenario, the abandonment of traditional land management practices, honed over centuries to adapt to the harsh desert environment, potentially leaves the oasis vulnerable to further degradation.

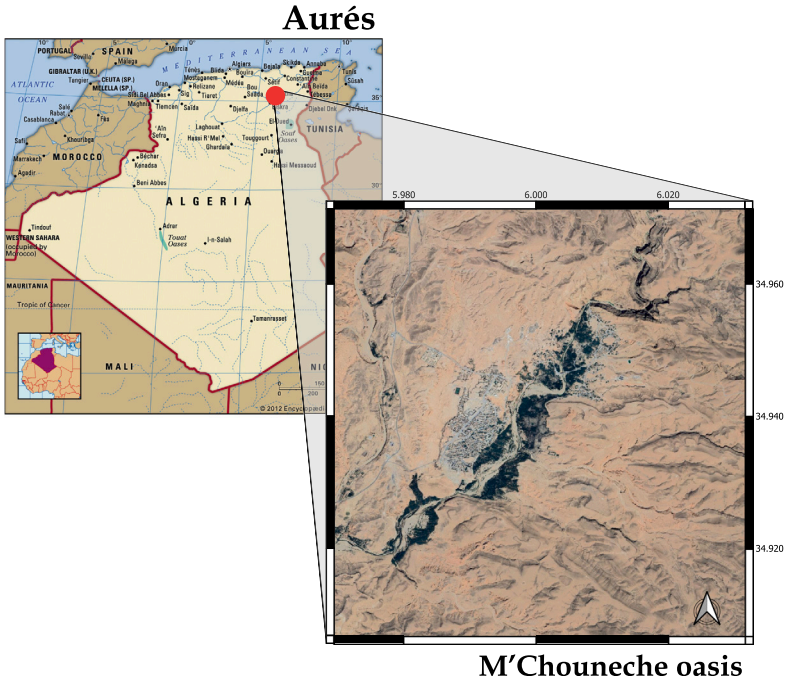

Fig. 1. Study area: Oasis of M'Chouneche, Aurès region (Algeria).

Fig. 2. M'Chouneche oasis.

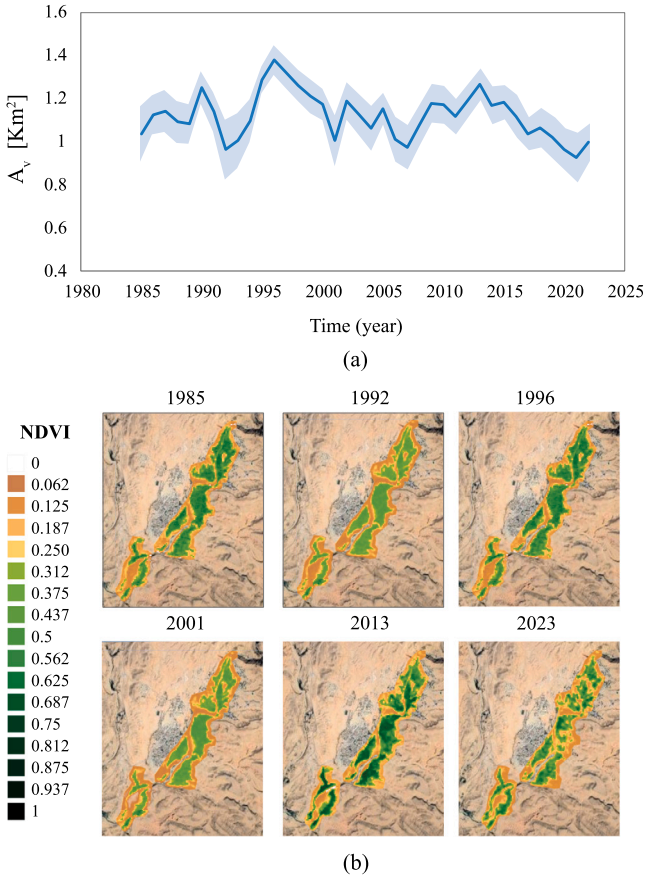

Fig. 3. Variation of the mean annual vegetative surface cover of the oasis A_v estimated from NDVI values (a): the shaded area corresponds to the envelope of A_v for $\tau^* = \tau^*_{min}$ and $\tau^* = \tau^*_{max}$, while the thick line is the mean A_v. Panel (b) shows the mean annual NDVI spatial distribution for some selected years.

4. Results

The results are organized following the primary objectives of the study, as outlined in Section 2. Section 4.1 details the assessment of changes in the oasis' vegetative surface cover. Statistical modeling of the time series for physical quantities is provided in Section 4.2.

4.1. Assessment of the oasis's vegetative surface changes

The extension of vegetative cover within the M'Chouneche oasis is investigated by satellite imagery analysis. The optimal threshold value for the NDVI was determined by comparing Landsat 8 and Sentinel 2 satellite images on a monthly basis from 2016 to 2023, as detailed in Section 2.2. The application of the proposed procedure and NDVI threshold identification are detailed in Section S1 of the Supplementary Material.

Fig. 3(a) depicts the temporal variation of the mean annual vegetative surface area (thick line). This value is calculated as the annual average of the vegetative area A_v derived from each available satellite image. The figure reveals fluctuations in the oasis area over the years, with three distinct periods of decline: 1990–1992, 1996–2001, and 2013–2023. Notably, the most recent period (2013–2023) exhibits a decrease in A_v of approximately 20%, potentially coinciding with the observed mortality of a significant number of palm trees. Fig. 3(b) presents mean annual NDVI maps for selected years of particular interest within the oasis. A clear correlation is evident between higher NDVI values and years with greater vegetative cover, indicating a denser plant population.

We further analyzed NDVI data focusing on the periods 1996–2001 and 2013–2023, which exhibited significant decreases in the mean annual vegetative surface area. Fig. 4(a) displays the spatial distribution of the vegetative decline in these periods obtained by comparing the vegetative masks extracted from the NDVI analysis at the end and at the beginning of the two time windows. For the period 1996–2001, the reduction primarily occurs in the oasis' northern region, while the central region appears more affected during the later interval 2013–2023. Fig. 4(b) presents the temporal variations of NDMI for regions with (red line) and without (black line) vegetation loss. The NDMI values are obtained by averaging the index values across pixels within the designated zones. Notably, regions experiencing vegetation loss exhibited lower and decreasing NDMI values compared to other areas. This trend is

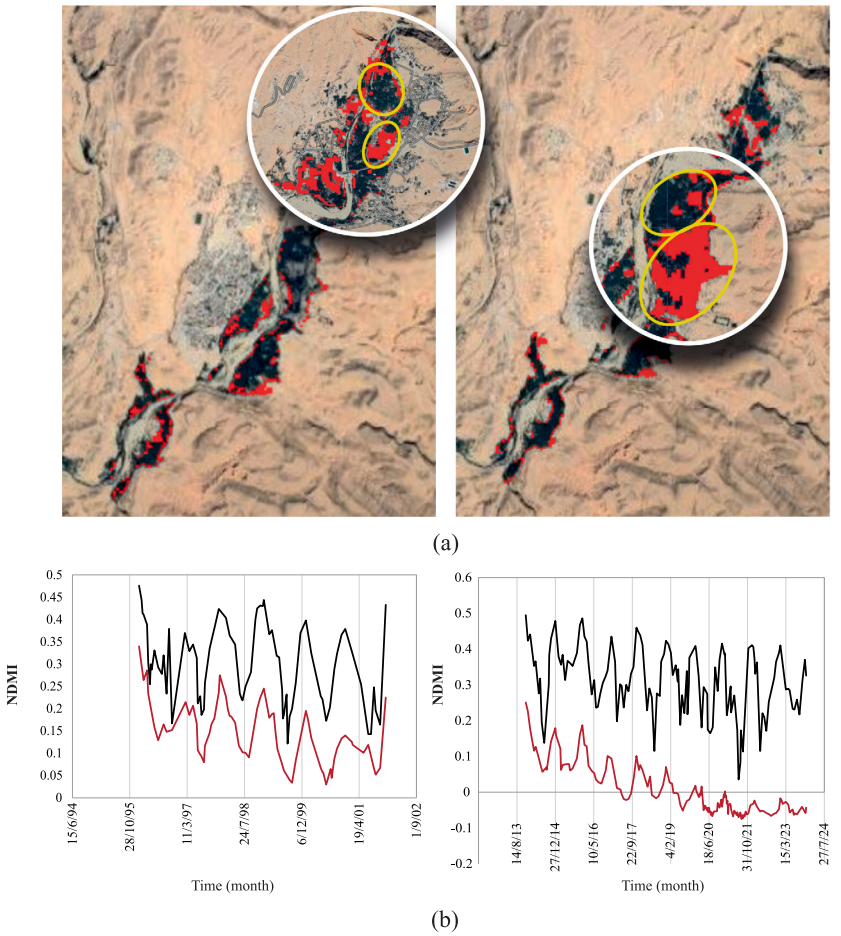

Fig. 4. Analysis of vegetation loss and water stress. (a) Areas with missing vegetative cover (red) during 1996–2001 (left) and 2013–2023 (right). (b) Mean NDMI of water-stressed (red line) and non-stressed areas (black line) indicated in the highlighted areas in (a).

particularly evident in the last decade, where a significant decrease in the NDMI is observed in the affected regions leading to the occurrence of a negative average NDMI. These findings suggest that the analyzed areas endured consecutive periods of water stress, potentially contributing to plant mortality due to climatic or water supply limitations.

4.1.1. Transferability to proximal oases

The methodology for estimating vegetative cover outlined in Section 2.2 relies on the definition of specific thresholds. To test the transferability of these thresholds to proximal oases, the procedure is here applied to two additional oases along the Wadi Abiod (Oued el Abiod Wadi). These oases, Baniane and Ghoufi, are located a few dozen kilometers north of M'Chouneche, as depicted in Fig. 5, and are characterized by the presence of palm groves. This analysis serves two primary purposes: (1) to assess changes in vegetation cover within these oases close to M'Chouneche and identify potential similarities in their vegetative dynamics compared to the studied case, (2) to evaluate the transferability of the proposed procedure to other proximal traditional oasis systems. The estimate of A_v is performed using the range of NDVI values ($\tau^* = \tau^*_{min}$ and $\tau^* = \tau^*_{max}$) both determined by applying the procedure outlined in Section 2.2 to the satellite images of the Baniane and Ghoufi oases and using the NDVI range optimized for M'Chouneche. The analysis is performed from 2013 to 2023, corresponding to the time frame where a significant reduction of the vegetation cover is observed in M'Chouneche. Fig. 5 reveals a decrease in vegetative cover at Baniane and Ghoufi oases. Details on calibrating the NDVI threshold for these additional oases are provided in Section S1.1 in Supplementary Material. For Ghoufi, the NDVI range estimated for M'Chouneche (red lines in Fig. 5) overestimates the mean annual vegetation cover by about 10% compared to the direct application of the procedure to the satellite images (blue line in Fig. 5). This can be attributed to the higher variability of the estimated optimal NDVI threshold in Ghoufi, possibly caused by the satellite image resolution being insufficient for the small oasis size. For Baniane, while the employed NDVI ranges show a similar decreasing trend, the A_v estimates obtained using the $\tau^* = \tau^*_{min}$ and $\tau^* = \tau^*_{max}$ values from Section 4.1 are on average 14% lower than their counterparts. This difference arises from the site-specific optimal NDVI threshold having a smaller variation and being slightly lower than the one obtained for M'Chouneche.

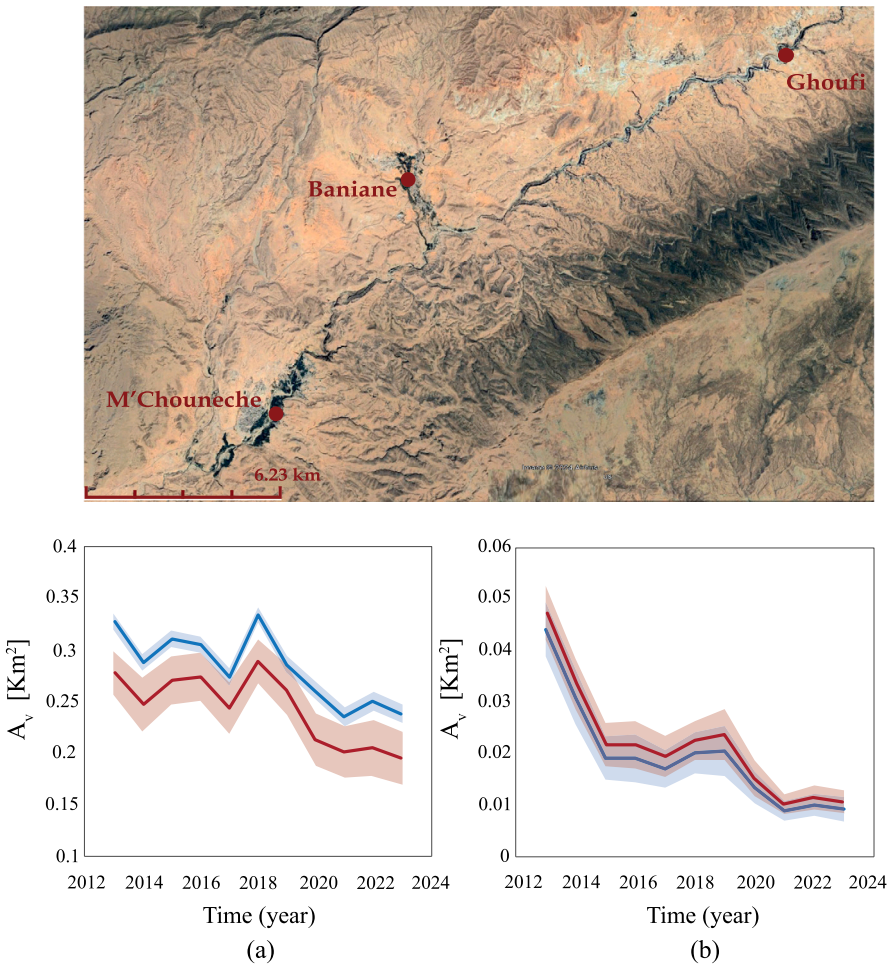

Fig. 5. Estimate of the vegetative cover of Baniane (a) and Ghoufi (b) oasis. Comparison of the area estimated by using the NDVI threshold values obtained for M'Chouneche oasis (red line) and applying the calibration procedure to the satellite images of the other oases (blue line). The shaded area corresponds to the envelope of A_v for $\tau^* = \tau^*_{min}$ and $\tau^* = \tau^*_{max}$, while the thick line is the mean A_v. (For interpretation of the references to color in this figure legend, the reader is referred to the web version of this article.)

The geographical and physical characteristics of the two oases may contribute to this variation in NDVI threshold values. In spite of these minor differences, all predictions display a similar decreasing trend, indicating that our methodology can be employed to analyze emerging trends in proximal systems without the need of re-calibrating the thresholds.

4.2. Modeling time series and future predictions

The climatic data and the results from the analysis of vegetative cover dynamics and water stress are used as input data for statistical modeling, employing the tools in Section 2.4.

4.2.1. Monthly data

Considering monthly data, the Augmented Dickey–Fuller test results in Section S1 indicate that all the assessed endogenous variables are stationary at level. Therefore, the VAR model is employed as an interpretive model. The VAR model can incorporate constant terms, trends, or seasonal components depending on the dataset characteristics (see Eq. (8)). We evaluated different VAR models and performed the diagnostic tests described in Section 2.5 to select the most suitable one. For the comparison, we consider the number of lags (q) providing the lowest AIC value for each model.

Table 2 reveals that including seasonality improves model performance. All seasonal VAR models have lower AIC values and perform better than others, especially in terms of stability. The significance of the seasonality is also supported by the autocorrelation function (ACF) plots of the endogenous variables (see Figure S4 in Supplementary Material). These plots show periodic patterns in the significant lags, especially for temperature and evapotranspiration data where a strong seasonality is observed.

Table 2
Comparison of different VAR models with and without seasonality: no constant and no trend term (None), with constant term (Const), with trend (Trend), with constant and trend term (Const+Trend). The results of the serial correlation, Heteroskedasticity, and normality are expressed in p-value.

Type	Seasonality	q	AIC	Stability (roots)	Serial correlation	Heteroskedasticity (ARCH)	Normality (JB)	Structural breaks
None	✗	9	882	≈ 1	0.0017	0.42	0.7764	✓
None	✓	3	840	> 1	0.24	0.63	0.008	✓
Const	✗	5	882	≈ 1	0.17	0.59	0.02	✓
Const	✓	2	827	< 1	0.25	0.42	0.001	✗
Const	✓	3	833	< 1	0.41	0.76	0.006	✓
Trend	✗	9	886	≈ 1	0.001	0.54	0.83	✓
Trend	✓	3	843	≈ 1	0.30	0.58	0.001	✓
Const+Trend	✗	5	881	≈ 1	0.20	0.64	0.071	✓
Const+Trend	✓	2	817	< 1	0.30	0.28	0.001	✓

Table 3
RMSE between the predicted and observed cumulative precipitation P_{cm}, mean temperature T_m and evapotranspiration ET_{0_m}, and oasis'area subjected to water stress R_{ws} for Model 1 and Model 2.

	P_{cm}	T_m	ET_{0_m}	R_{ws}
Model 1	9.80	1.64	0.73	0.04
Model 2	10.71	1.51	0.81	0.06

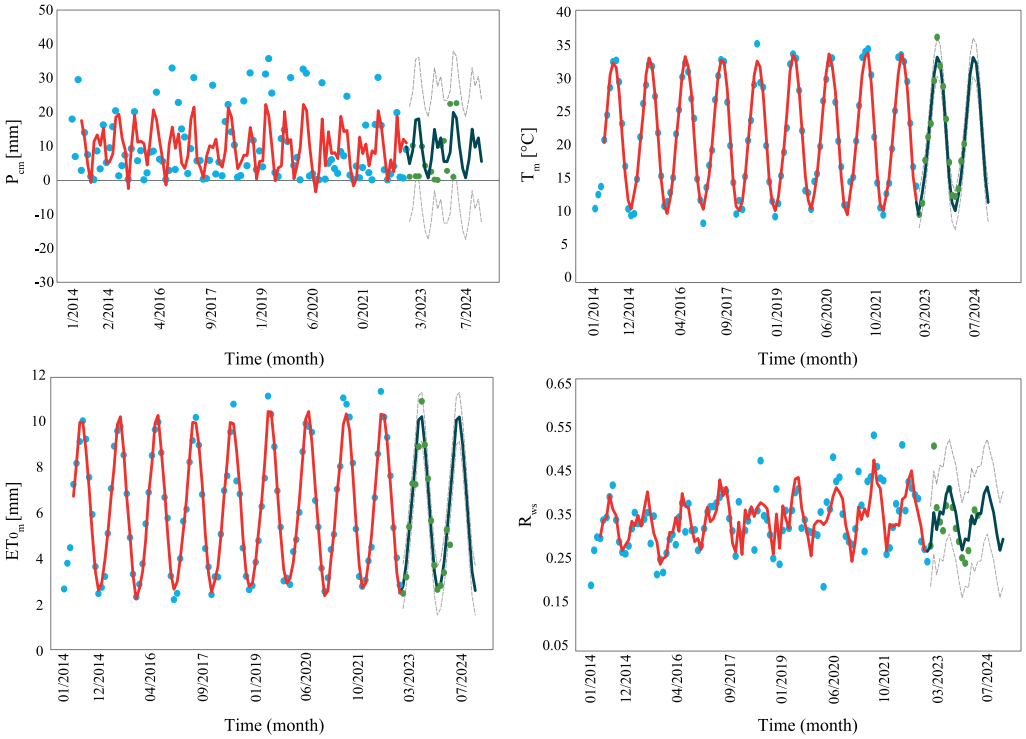

Fig. 6. Comparison of the fitted (solid red line) and predicted (solid black line) values of VAR Model 1 and the corresponding observations for the endogenous variables P_{cm}, T_m, ET_{0_m}, R_{ws}. The observation dataset is split into model calibration data (light blue markers) and model validation data (green markers). The dashed gray lines represent the upper and lower 95% confidence bounds. (For interpretation of the references to color in this figure legend, the reader is referred to the web version of this article.)

Table 2 reveals two strong contenders for the best performing model: Model 1 (constant term only) and Model 2 (constant and trend terms). Both achieve the lowest AIC values and satisfy the diagnostic tests, with the exception of the normality test which is not a strict requirement. To determine the most suitable model, we assessed their 16-step-ahead predictions against actual observations of the target variables. Root Mean Square Error (RMSE) is used as metric for evaluating prediction accuracy. As shown in Table 3, Model 1 outperforms Model 2 in terms of RMSE, except for the variable T_m, and therefore is chosen as the reference VAR model.

As displayed in Fig. 6, Model 1 provides a good match between (1) the fitted values and the observations over the time range from 2014 to 2022 and (2) the predicted values and the reference observed data for 2023–2024. Lower accuracy is observed in the predictions/estimates of the monthly cumulative precipitation, as compared to the other variables.

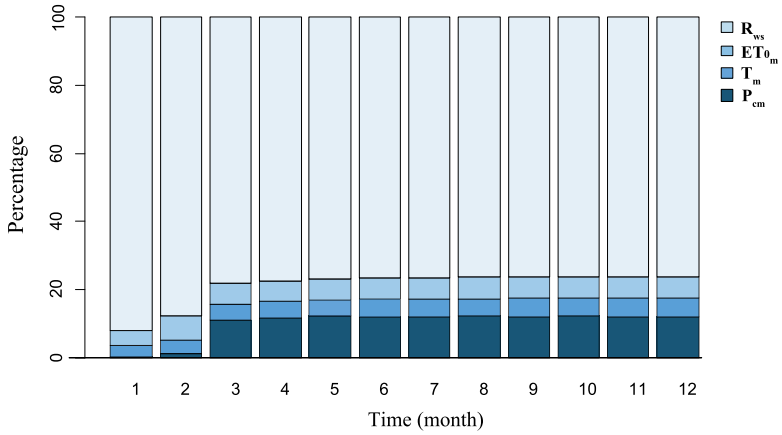

Fig. 7. FEVD for the water stressed area R_{ws}.

Table 4
Posterior probability of the candidates VEC models: type of cointegration term (without additional term (none), with constant term (const), with trend term (trend)), number of lags q, AIC value associated to the VEC model, posterior probability $p(M_k \mid \mathbf{X}^*)$.

	Cointegration term	q	AIC	$p(M_k \mid \mathbf{X}^*)$
Model_n	none	5	−202.09	0.03
Model_c	constant	5	−208.84	0.96
Model_t	trend	4	−139.42	8.15×10^{-16}

VAR Model 1 is then employed to assess the correlation between the variables, particularly focusing on the oasis's area subjected to water stress R_{ws}. The 96 estimated model coefficients, obtained by OLS methods, are reported in Table S9 in Supplementary Material.

The FEVD analysis in Fig. 7 shows the contribution of each variable to the forecast error variance of R_{ws} over 12 time steps ahead. Notably, R_{ws} itself has the strongest influence, with a peak impact of 90% in the first step. Temperature and evapotranspiration contribute a minor and relatively constant 5% each, while precipitation becomes increasingly significant after the first step, reaching 12% by the fourth step. This suggests a lagged effect of P_{cm} on R_{ws} probably associated with soil water retention and variation of water content. The lagged effect helps explain why consecutive periods of water stress can lead to the loss of vegetative cover observed in Figs. 3 and 4.

4.2.2. Annual data

Climate change and its impact on the oasis vegetative cover are assessed by analyzing the annual climatic data, in terms of cumulative precipitation P_{ca}, mean temperature T_a and evapotranspiration ET_{0a}, and the vegetative cover A_v for a period of 38 years. As displayed in Fig. 8, the observed climatic data (light blue dots) reveal a reduction in annual cumulative precipitation and an increase in annual mean temperature and evapotranspiration, becoming more pronounced after 2005.

The Augmented Dickey–Fuller test results indicate that our annual endogenous variables are non-stationary in levels, but become stationary at first difference (see Table S2 of Supplementary Material). Moreover, the Johansen test (see Table S3 in Supplementary Material) reveals the existence of two cointegrations, i.e. long-term equilibrium relationships, between the variables. Thus, the time series meets the requirements for the application of the VEC model.

The cointegration term within the VEC model in Eq. (9) may include a constant or a trend component, alongside the β coefficient. In this term, we evaluate different VEC models, with and without this additional term (constant or trend) in the cointegration relationship. For each model, we compute the posterior probability using the AIC index, according to Eq. (7). Due to the limited amount of available annual data, model selection relies on the posterior probability rather than the RMSE between predicted and observed future values, as employed for the monthly data in Section 4.2.1. As indicated in Table 4, the VEC model incorporating a constant term in the cointegration relationship (Model_c) exhibits the highest posterior probability, which aligns with the highest AIC value. Model_t provides the greatest AIC values and the lowest posterior probability. The estimated coefficients for Model_c (88 in total, comprising the cointegration and lag term coefficients) are provided in Table S5 in the Supplementary Material. Moreover, the model satisfied the suitability test in terms of stability, residual autocorrelation, heteroskedasticity, and normality (see Table S7 in Supplementary Material).

The estimated posterior probability is then employed to compute model predictions by averaging the model outputs using the $p(M_k \mid \mathbf{X}^*)$ value, as reported in Eq. (7). As shown in Fig. 8, the resulting VEC prediction effectively approximates the observed endogenous variables from 1991 to 2022. The RMSE between the model results and observed values is equal to 20.67 mm, 0.29 °C, 0.10 mm, 0.029 km^2 for P_{ca}, T_a, ET_{0a}, and A_v, respectively.

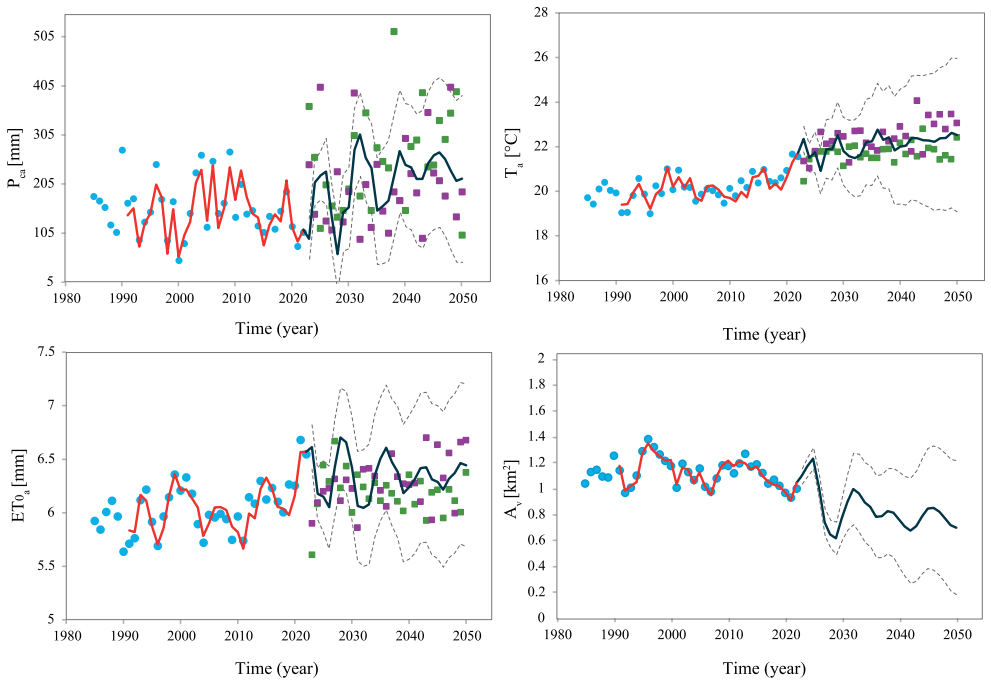

Fig. 8. Comparison between (1) the VEC model fitting (red line) and the observations (light blue dots) and (2) the VEC model predictions (dark blue line) and the NEX-GDDP-CMIP6 predictions (magenta squared markers (SSP5-8.5 scenario) and green squared markers (SSP2-4.5 scenario)). The dashed gray lines represent the upper and lower 95% confidence bounds. (For interpretation of the references to color in this figure legend, the reader is referred to the web version of this article.)

We extend our predictions until 2050 to gain insights on the possible future trajectory of the oasis system. The uncertainty associated with these predictions is also considered and reported in Fig. 8. The averaged predictions for P_{ca} reveal a rising trend with an average growth of approximately 87 mm. An increase is also expected in the annual mean temperature and evapotranspiration.

The VEC model predictions are compared with climate change projections from NEX-GDDP-CMIP6, specifically the SSP2-4.5 (Middle Road) and SSP5-8.5 (Fossil-Fuel Development) scenarios which consider global economic and demographic changes as well as greenhouse gas emissions (Fu et al., 2023). The SSP2-4.5 scenario represents the medium pathway of future greenhouse gas emissions and incorporates climate change mitigation efforts. The SSP5-8.5 scenario assumes high emissions without significant mitigation efforts mimicking an economic development based on an intensified exploitation of fossil fuel resources. As shown in Fig. 8, the SSP5-8.5 scenario predicts harsher climatic conditions for the oasis with lower annual cumulative precipitation and higher annual mean temperature and evapotranspiration compared to SSP2-4.5. The VEC predictions align well with the NEX-GDDP-CMIP6 projections, particularly for temperature and evapotranspiration. Predicted precipitations display some mismatch, yet the NEX-GDDP-CMIP6 projections mostly fall within the confidence range of the VEC model predictions. Overall, the VEC predictions lean closer to the SSP5-8.5 scenario.

The VEC model predicts a reduction in the oasis' vegetative surface. This translates to an expected decrease of around 36% by 2050 under the projected climate change scenario and without mitigation efforts. This highlights the urgent need for interventions to improve water resource management and agricultural practices.

Results reported in Fig. 8 assume the oasis vegetative surface cover to be a deterministic input. To consider the uncertainty associated with the estimate of the vegetative surface cover determined in Section 4.1, we sampled 100 realizations of A_v time series. To this end for each year we randomly select a value from a uniform distribution on the interval $[A_v(\tau^*_{max}), A_v(\tau^*_{min})]$. These realizations represent the potential variation in vegetative surface based on the uncertainty in the NDVI threshold. For each realization, we use the VEC model to generate future projections and to obtain the envelope of realizations quantifying the uncertainty associated with A_v. As displayed in Fig. 9, the envelope of model realizations mostly predicts a vegetative surface decline. The reference projection (red dashed line), which is obtained when considering the average value of $[A_v(\tau^*_{max}), A_v(\tau^*_{min})]$, represents a scenario close to the 75th percentile of A_v realizations.

5. Discussion and conclusions

Our work focuses on understanding the relationship between climatic factors and vegetation dynamics in traditional oases. We employ remote sensing data and data-driven models to evaluate the historical and projected trajectory of traditional oasis systems, providing evidence of oasis vegetative cover dynamics over time and inferring future trends. Key innovations include

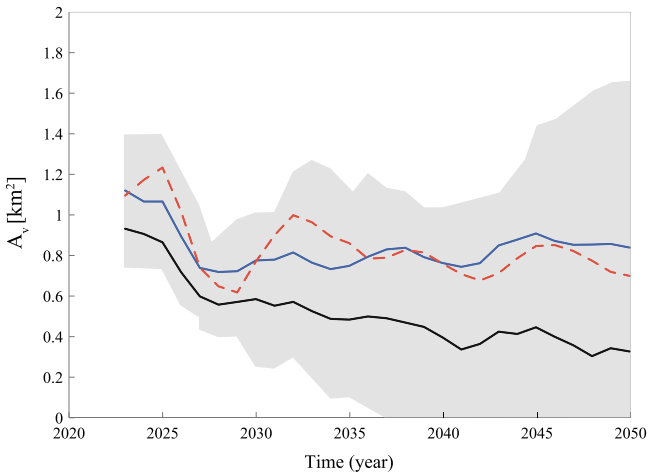

Fig. 9. Sample of VEC model predictions for the vegetative surface cover A_v including the uncertainty on A_v estimate: reference prediction obtained employing the average value of $[A_v(\tau^*_{max}), A_v(\tau^*_{min})]$(red dashed line), 25th (black line) and 75th (blue line) percentile of the A_v realizations. The shaded area represents the envelope corresponding to the whole sample of A_v realizations. (For interpretation of the references to color in this figure legend, the reader is referred to the web version of this article.)

a robust methodology for assessing oasis area using NDVI and NDMI indices from Landsat and Sentinel imagery. Additionally, we introduce and benchmark VAR and VEC models to analyze water stress and vegetative surface cover dynamics through probabilistic approaches. Our analysis considers climatic variables' impact, in terms of precipitation, temperature, and evapotranspiration, on oasis vegetation at both monthly (VAR) and annual (VEC) scales.

The methodology is applied to the M'Chouneche oasis in the Aurés area, Algeria, in line with the objectives of the AMAZING project. Analysis of satellite imagery revealed a decline in oasis vegetation cover, particularly in the past decade, with a decrease of approximately 20%. This trend was also observed in other oases in the same watershed (i.e., the Baniane and Ghoufi oases). Our method to estimate oasis area requires the estimation of optimal thresholds, which are in principle site-specific. Yet, our results document that the estimated thresholds can be transferred to proximal oases. When comparing the estimated cover using the NDVI threshold derived specifically for each oasis versus the threshold obtained from M'Chouneche, we observed discrepancies of approximately 10% and 14% for Ghoufi and Baniane oases, respectively. These variations likely stem from differences in image resolution relative to oasis size, along with geographical and physical characteristics of each oasis. Broad application in other geographical contexts is left for future works and is beyond the scope of this work.

The VAR model demonstrates good accuracy in both modeling and predicting future values of the assessed climatic and vegetative variables at the monthly timescale. The results indicate that among the climatic drivers, cumulative precipitation has the most significant impact on plant water stress, with a lagged effect. This behavior may explain why consecutive periods of water stress can lead to the observed palm tree mortality. Shifting to the annual scale, the VEC model exhibits good accuracy in modeling the interaction between climate change and vegetative cover dynamics. The model projections for climatic variables obtained from our data-driven approaches closely align with the NEX-GDDP-CMIP6 climate change projections. The VEC model suggests a significant reduction in vegetative cover by 2050. This outcome underscores the importance of strategic interventions, such as improved water resource management, to preserve traditional oases and prevent desertification and abandonment.

CRediT authorship contribution statement

Elisa Baioni: Writing – original draft, Visualization, Validation, Software, Methodology, Investigation, Data curation, Conceptualization. **Giulia Fiantanese:** Writing – review & editing, Methodology, Data curation, Conceptualization. **Giovanni Michele Porta:** Writing – review & editing, Supervision, Methodology, Investigation, Funding acquisition, Conceptualization.

Funding

The authors acknowledge the funding received by Politecnico di Milano, Italy under the Polisocial 2022 call. We acknowledge the invaluable support from Prof. S. Guergazi, B. Guerira, N. Belghar (University of Biskra) and Prof. R. Attoui (University of Annaba) to the AMAZING project.

Declaration of competing interest

The authors declare that they have no known competing financial interests or personal relationships that could have appeared to influence the work reported in this paper.

Appendix A. Supplementary data

Supplementary material related to this article can be found online at https://doi.org/10.1016/j.ejrh.2025.102266.

Data availability

Data and codes used to generate results are available through data repository https://data.mendeley.com/preview/gcx5hkfb5k?a=07bddc9c-f3db-47c9-823c-894d869c8232.

References

Adenomon, M.O., Ojehomon, V.E., Oyejola, B.A., 2013. Modelling the dynamic relationship between rainfall and temperature time series data in niger state, Nigeria. Math. Theory Model. 3, 53–70, URL: https://api.semanticscholar.org/CorpusID:64358324.

Al-Gaadi, K., Hassaballa, A., Tola, E., Kayad, A., Madugundu, R., Alblewi, B., Assiri, F., 2016. Prediction of potato crop yield using precision agriculture techniques. PLoS ONE 11, http://dx.doi.org/10.1371/journal.pone.0162219.

AMAZING, 2023. Amazing project. URL: https://www.amazing.polimi.it.

Awokuse, T.O., Bessler, D.A., 2003. Vector autoregressions, policy analysis, and directed acyclic graphs: an application to the US economy. J. Appl. Econ. 6 (1), 1–24. http://dx.doi.org/10.1080/15140326.2003.12040583.

Banerjee, A., Dolado, J.J., Galbraith, J.W., Hendry, D., 1993. Co-Integration, Error Correction, and the Econometric Analysis of Non-Stationary Data. Oxford University Press.

Boori, M., Choudhary, K., Kupriyanov, A., 2020. Crop growth monitoring through sentinel and landsat data based NDVI time-series. Comput. Opt. 44, 409–419. http://dx.doi.org/10.18287/2412-6179-co-635.

Breusch, T.S., 1978. Testing for autocorrelation in dynamic linear models. Aust. Econ. Pap. 17 (31), http://dx.doi.org/10.1111/j.1467-8454.1978.tb00635.x.

Chen, Y., Fang, G., Li, Z., Zhang, X., Gao, L., Elbeltagi, A., Shaer, H.E., Duan, W., Wassif, O.M.A., Li, Y., Luo, P., Selmi, A., Yu, R., Yang, J., Hu, Y., Liu, C., Long, Y., Malik, I., Fu, A., Wistuba, M., Yang, Y., Zhu, C., Gao, Y., 2024. The crisis in oases: Research on ecological security and sustainable development in arid regions. Annu. Rev. Environ. Resour. http://dx.doi.org/10.1146/annurev-environ-111522-105932.

Clements, M.P., Mizon, G., 1991. Empirical analysis of macroeconomic time series : VAR and structural models. Eur. Econ. Rev. 35, 887–917. http://dx.doi.org/10.1016/0014-2921(91)90042-H.

Copernicus, C.C.S., 2017. ERA5 Ag: Agrometeorological Indicators from 1979 to Present Derived from Reanalysis. Copernicus Climate Change Service Climate Data Store (CDS), URL: https://cds.climate.copernicus.eu/cdsapp#!/dataset/sis-agrometeorological-indicators?tab=overview.

Dechoz, C., Poulain, V., Massera, S., Languille, F., Greslou, D., De Lussy, F., Gaudel, A., L'Helguen, C., Picard, C., Trémas, T., 2015. Sentinel 2 global reference image. In: Image and Signal Processing for Remote Sensing XXI, vol. 9643, SPIE, pp. 94–107. http://dx.doi.org/10.1117/12.2195046.

Dhawi, F., Aleidan, M.M., 2024. Oasis agriculture revitalization and carbon sequestration for climate-resilient communities. Front. Agron. 6, http://dx.doi.org/10.3389/fagro.2024.1386671.

Edgerton, D., Shukur, G., 1999. Testing autocorrelation in a system perspective testing autocorrelation. Econometric Rev. 18 (4), 343–386. http://dx.doi.org/10.1080/07474939908800351.

Fahria, I., Sulistiana, I., 2021. Vector error correction model to analyze energy uses, environmental quality and economic growth during Covid-19 Pandemic. IOP Conf. Series: Earth Environ. Sci. 926, http://dx.doi.org/10.1088/1755-1315/926/1/012066.

Ferdous, M., Baten, M., et al., 2011. Climatic variables of 50 years and their trends over Rajshahi and Rangpur division. J. Environ. Sci. Nat. Resour. 4 (2), 147–150. http://dx.doi.org/10.3329/jesnr.v4i2.10165.

Fiantanese, G., 2023. Water and Soil Dynamics in the Aurès region. (Master's thesis). Politecnico di Milano, URL: https://hdl.handle.net/10589/204736.

Filgueiras, R., Mantovani, E., Althoff, D., Filho, E.F., Cunha, F.F., 2019. Crop NDVI monitoring based on sentinel 1. Remote. Sens. 11, 1441. http://dx.doi.org/10.3390/RS11121441.

Fu, Y., Zhuang, H., Shen, X., Li, W., 2023. Assessment and prediction of regional climate based on a multimodel ensemble machine learning method. Clim. Dyn. 61 (9), 4139–4158. http://dx.doi.org/10.1007/s00382-023-06787-7.

Gao, B.-c., 1996. NDWI—A normalized difference water index for remote sensing of vegetation liquid water from space. Remote Sens. Environ. 58 (3), 257–266. http://dx.doi.org/10.1016/S0034-4257(96)00067-3.

Hamilton, J.D., 2020. Time Series Analysis. Princeton University Press.

Hayes, D.J., Cohen, W.B., Sader, S.A., Irwin, D.E., 2008. Estimating proportional change in forest cover as a continuous variable from multi-year MODIS data. Remote Sens. Environ. 112 (3), 735–749. http://dx.doi.org/10.1016/j.rse.2007.06.003.

Honkatukia, J., Mälkönen, V., Perrels, A., 2008. Impacts of the European emissions trading scheme on finnish wholesale electricity prices. In: Markets for Carbon and Power Pricing in Europe. Edward Elgar Publishing, http://dx.doi.org/10.4337/9781848445031.00013.

Huang, S., Tang, L., Hupy, J.P., Wang, Y., Shao, G., 2021. A commentary review on the use of normalized difference vegetation index (NDVI) in the era of popular remote sensing. J. For. Res. 32 (1), http://dx.doi.org/10.1007/s11676-020-01155-1.

Ihlen, V., 2019. Landsat 8 (L8) data users handbook. URL: https://www.usgs.gov/media/files/landsat-8-data-users-handbook. LSRD Project Manager, LSDS CCB Chair.

Isioye, O., Akomolafe, E.A., Ikwueze, U.H., 2020. Accuracy analysis of sentinel 2a and landsat 8 oli+ satellite datasets over Kano state (Nigeria) using vegetation spectral indices. ISPRS - Int. Arch. Photogramm. Remote. Sens. Spat. Inf. Sci. 65–72. http://dx.doi.org/10.5194/isprs-archives-xliv-3-w1-2020-65-2020.

Janetti, E.B., Dror, I., Guadagnini, A., Riva, M., Berkowitz, B., 2012. Estimation of single-metal and competitive sorption isotherms through maximum likelihood and model quality criteria. Soil Sci. Am. J. 76 (4), 1229–1245. http://dx.doi.org/10.2136/sssaj2012.0010.

Johansen, S., 1988. Statistical analysis of cointegration vectors. J. Econom. Dynam. Control 12 (2–3), 231–254. http://dx.doi.org/10.1016/0165-1889(88)90041-3.

Johansen, S., Juselius, K., 1990. Maximum likelihood estimation and inference on cointegration–with applications to the demand for money. Oxf. Bull. Econ. Stat. 52 (2), 169–210. http://dx.doi.org/10.1111/j.1468-0084.1990.mp52002003.x.

Kaur, H., Alam, M.A., Mariyam, S., Alankar, B., Chauhan, R., Adnan, R., Kisi, O., 2021. Predicting water availability in water bodies under the influence of precipitation and water management actions using VAR/VECM/lstm. Climate http://dx.doi.org/10.3390/cli9090144.

Kleiber, A., 2002. An {R} package for testing for structural change in linear regression models. An {R} Packag. Test. Struct. 7 (2).

Kleiber, W., Katz, R.W., Rajagopalan, B., 2013. Daily minimum and maximum temperature simulation over complex terrain. Ann. Appl. Stat. 7 (1), 588–612. http://dx.doi.org/10.1214/12-AOAS602.

Levin, N., Shmida, A., Levanoni, O., Tamari, H., Kark, S., 2007. Predicting mountain plant richness and rarity from space using satellite-derived vegetation indices. Diversity and Distributions 13, http://dx.doi.org/10.1111/j.1472-4642.2007.00372.x.

Li, C., Li, H., Li, J., Lei, Y., Li, C., Manevski, K., Shen, Y., 2019. Using NDVI percentiles to monitor real-time crop growth. Comput. Electron. Agric. 162, 357–363. http://dx.doi.org/10.1016/J.COMPAG.2019.04.026.

Lin, M.-L., Chen, C.-W., yi Shih, J., Lee, Y.-T., Tsai, C.-H., Hu, Y.-T., Sun, F., Wang, C.-Y., 2009. Using MODIS-based vegetation and moisture indices for oasis landscape monitoring in an arid environment. 2009 IEEE Int. Geosci. Remote. Sens. Symp. 4, http://dx.doi.org/10.1109/IGARSS.2009.5417382, IV–338–IV–341.

Lin, M.-L., Chu, C.-M., Tsai, B., 2011. Drought risk assessment in western inner-mongolia. Int. J. Environ. Res. 5, 139–148. http://dx.doi.org/10.22059/IJER.2010.299.

Liu, C., Yan, X., Jiang, F., 2021. Desert vegetation responses to the temporal distribution patterns of precipitation across the northern Xinjiang, China. CATENA 206, 105544. http://dx.doi.org/10.1016/j.catena.2021.105544.

Lütkepohl, H., 2005. New Introduction to Multiple Time Series Analysis. Springer Science & Business Media.

Lütkepohl, H., 2013. Vector autoregressive models. In: Handbook of Research Methods and Applications in Empirical Macroeconomics. Edward Elgar Publishing, pp. 139–164.

Medouki, M., Mezerdi, T., Sfaksi, I., 2022. Natural daylighting in traditional architecture: A case study of courtyard houses in the Oasis city of M'chouneche, Algeria. Int. J. Innov. Stud. Sociol. Humanit. http://dx.doi.org/10.20431/2456-4931.070912.

Mo, K., Chen, Q., Chen, C., Zhang, J., Wang, L., Bao, Z., 2019. Spatiotemporal variation of correlation between vegetation cover and precipitation in an arid mountain-Oasis river basin in Northwest China. J. Hydrol. 574, 138–147. http://dx.doi.org/10.1016/j.jhydrol.2019.04.044.

Muñoz Sabater, J., 2019. ERA5-land monthly averaged data from 1981 to present, Copernicus Climate Change Service (C3S) Climate Data Store (CDS)[data set]. http://dx.doi.org/10.24381/cds.68d2bb30.

Nuruzzaman, M., Soni, M.S.M., Rana, M.S., Hossain, M.S., Molla, M.M.R., et al., 2023. Forecasting climatic variables using vector autoregression (VAR) model. Eur. J. Stat. Probab. 11 (1), 20–38. http://dx.doi.org/10.37745/ejsp.2013/vol11n12038.

Otsu, N., et al., 1975. A threshold selection method from gray-level histograms. Automatica 11 (285–296), 23–27.

Petit, O., Kuper, M., López-Gunn, E., Rinaudo, J.-D., Daoudi, A., Lejars, C., 2017. Can agricultural groundwater economies collapse? An inquiry into the pathways of four groundwater economies under threat. Hydrogeol. J. 25 (6), 1549–1564. http://dx.doi.org/10.1007/s10040-017-1567-3.

Pfaff, B., Taunus, K., 2007. Using the vars package. Kronberg: Im Taunus 2007.

R. Core Team, et al., 2016. R: A language and environment for statistical computing. R foundation for statistical computing, Vienna, Austria. http://www.R-project.org/.

Rouse, Jr., J.W., Haas, R.H., Schell, J., Deering, D., 1973. Monitoring the Vernal Advancement and Retrogradation (Green Wave Effect) of Natural Vegetation. Technical Report, Texas A&M Univ.College Station, TX, United States, https://ntrs.nasa.gov/citations/19750020419.

Sakamoto, Y., Ishiguro, M., Kitagawa, G., 1986. Akaike information criterion statistics. Mathematics and Its Applications Japanese Series. (no. 1), Reidel, Dordrecht.

Santoro, A., 2023. Traditional Oases in Northern Africa as multifunctional agroforestry systems: a systematic literature review of the provided ecosystem services and of the main vulnerabilities. Agrofor. Syst. 97 (1), 81–96. http://dx.doi.org/10.1007/s10457-022-00789-w.

Sayler, K., 2020. Landsat 4-7 collection 1 (C1) surface reflectance (LEDAPS) product guide. URL: https://www.usgs.gov/media/files/landsat-4-7-collection-1-surface-reflectance-code-ledaps-product-guide. LSRD Project Manager.

Stephenson, D., Turasie, A., Cummins, D.P., 2023. More accurate climate trend attribution by using cointegrating vector time series models. Sustainability http://dx.doi.org/10.3390/su151612142.

Sudheesh, R., Subramanian, D., 2022. Multi-variate time-series analysis using VECM identifies the best set of exogenous predictors for rainfall and temperature in India: A data analytical approach. Asian J. Res. Comput. Sci. 14 (4), 166–174. http://dx.doi.org/10.9734/ajrcos/2022/v14i4300.

Thoenes, S., 2014. Understanding the determinants of electricity prices and the impact of the German nuclear moratorium in 2011. Energy J. 35 (4), 61–78. http://dx.doi.org/10.5547/01956574.35.4.3.

Thrasher, B., Maurer, E.P., McKellar, C., Duffy, P.B., 2012. Bias correcting climate model simulated daily temperature extremes with quantile mapping. Hydrol. Earth Syst. Sci. 16 (9), 3309–3314. http://dx.doi.org/10.5194/hess-16-3309-2012.

Wallace, J., Behn, G., Furby, S., 2006. Vegetation condition assessment and monitoring from sequences of satellite imagery. Ecol. Manag. Restor. 7, 31–36. http://dx.doi.org/10.1111/J.1442-8903.2006.00289.X.

Wilson, E.H., Sader, S.A., 2002. Detection of forest harvest type using multiple dates of Landsat TM imagery. Remote Sens. Environ. 80 (3), 385–396. http://dx.doi.org/10.1016/S0034-4257(01)00318-2.

Yu, F., Price, K., Ellis, J., Feddema, J., Shi, P., 2004. Interannual variations of the grassland boundaries bordering the eastern edges of the Gobi Desert in central Asia. Int. J. Remote Sens. 25, 327–346. http://dx.doi.org/10.1080/0143116031000084297.

Zotarelli, L., Dukes, M.D., Romero, C.C., Migliaccio, K.W., Morgan, K.T., 2010. Step by step calculation of the penman-Monteith evapotranspiration (FAO-56 method). Inst. Food Agric. Sci. Univ. Fla. 8, https://edis-ae459-2010.